Journal of Power Sources 342 (2017) 562–569

Contents lists available at ScienceDirect

Journal of Power Sources

journal homepage: www.elsevier.com/locate/jpowsour

In operando neutron diffraction study of the temperature and current rate-dependent phase evolution of $LiFePO_4$ in a commercial battery

N. Sharma [a, *], D.H. Yu [b], Y. Zhu [c], Y. Wu [c], V.K. Peterson [b, d]

[a] School of Chemistry, UNSW Australia, Sydney, NSW 2052, Australia
[b] Australian Centre for Neutron Scattering, Australian Nuclear Science and Technology Organisation, Locked Bag 2001, Kirrawee DC, NSW 2232, Australia
[c] College of Energy and Institute for Electrochemical Energy Storage, Nanjing Tech University, Nanjing 211816, Jiangsu Province, China
[d] Institute for Superconducting and Electronic Materials, Faculty of Engineering, School of Mechanical, Materials, and Mechatronic Engineering, University of Wollongong, NSW 2522, Australia

HIGHLIGHTS

- Non-equilibrium phase evolution determined by *in operando* neutron diffraction.
- Thermal and current processes significantly delays $LiFePO_4$ to $FePO_4$ transitions.
- $LiFePO_4$ to $FePO_4$ transitions occur in subsequent electrochemical steps.

ARTICLE INFO

Article history:
Received 22 September 2016
Received in revised form
25 November 2016
Accepted 12 December 2016
Available online 31 December 2016

Keywords:
Positive electrode
Rate of reactions
In situ neutron diffraction
Commercial batteries

ABSTRACT

In operando NPD data of electrodes in lithium-ion batteries reveal unusual $LiFePO_4$ phase evolution after the application of a thermal step and at high current. At low current under ambient conditions the $LiFePO_4$ to $FePO_4$ two-phase reaction occurs during the charge process, however, following a thermal step and at higher current this reaction appears at the end of charge and continues into the next electrochemical step. The same behavior is observed for the $FePO_4$ to $LiFePO_4$ transition, occurring at the end of discharge and continuing into the following electrochemical step. This suggests that the bulk (or the majority of the) electrode transformation is dependent on the battery's history, current, or temperature. Such information concerning the non-equilibrium evolution of an electrode allows a direct link between the electrode's functional mechanism that underpins lithium-ion battery behavior and the real-life operating conditions of the battery, such as variable temperature and current, to be made.

1. Introduction

The $LiCoO_2$ || graphite lithium-ion battery was commercialised in the 1990s [1] and has since been implemented in billions of portable electronic devices such as mobile phones and laptop computers [2]. $LiCoO_2$ is a costly and relatively-toxic positive electrode. Other positive electrode materials such as $LiMn_2O_4$ [3] and $LiFePO_4$ [4] have been developed to replace $LiCoO_2$ due to the higher relative abundance and lower toxicity of their constituent elements. Although $LiFePO_4$ is an intrinsically poor ionic conductor [4], efforts have been made to find ways to improve its performance, ranging from cation-doping [5,6] and nano-sizing [7] to carbon-coating [5,8,9].

The delithiation and lithiation reaction mechanisms of $Li_{1-x}FePO_4$ typically features a two-phase reaction over virtually the entire range of lithiation in the conventional case [4] (*i.e.* with relatively-large particle sizes and minimal Li/Fe antisite mixing [7]), although solid-solution domains are noted near the $LiFePO_4$ and $FePO_4$ end members. Additionally, particular particle morphology and defects can induce a wider solid-solution mechanism throughout the charge/discharge process [7,10–14]. Recent work revealed evidence of a current-dependent reaction mechanism, with high rates of charge/discharge featuring intermediate phases [15–17]. This work was performed using *in operando* powder diffraction experiments in which both time and angular resolution needed to be reasonable to identify intermediate phases.

In situ/operando neutron powder-diffraction (NPD) is being increasingly applied to commercial and custom made lithium-ion

* Corresponding author.
E-mail address: neeraj.sharma@unsw.edu.au (N. Sharma).

http://dx.doi.org/10.1016/j.jpowsour.2016.12.048
0378-7753/

batteries with studies investigating a range of positive and negative electrode materials [18–20], such as $LiCoO_2$ [21–25], $Li_{1+y}Mn_2O_4$ [26], graphite [24,27], and $Li_4Ti_5O_{12}$ [28–31] to name a few. Researchers have explored the current-rate dependency of phase transitions [21], overcharging or high voltage conditions [27,32,33] and associated fatigue processes [34], the function of large-format batteries [35], compared positive electrodes as a function of charge/discharge [23,36–39], and developed a variety of neutron-friendly cells that mimic the performance of commercial cells whilst providing a good NPD signal in *in situ/operando* experiments [6,28,29,40–45]. The limitations of NPD to explore lithium-ion batteries can include long collection times and insufficient angular-resolution, with the latter leading to the inability to accurately determine desired atomic parameters such as lithium site-occupancy factors (SOFs). Researchers are overcoming some or all of these hurdles as designs and methods continue to improve [46,47]. This is driven by the wealth of information that can be extracted from such *in situ/operando* data, which allows a direct link between empirically-optimised electrode performance and crystallographic structure to be made.

For $Li_{1-x}FePO_4$, *in situ* X-ray powder diffraction (XRPD) and *in situ* NPD experiments have revealed the transformation between $LiFePO_4$ and $FePO_4$ [48–50], but only a few show the time-dependence of this transformation (e.g. chemical delithiation [48]). Evidence of asymmetry in the kinetics of $FePO_4$ lithiation and $LiFePO_4$ delithiation has been demonstrated [12]. If the kinetics of these phase transformations can be determined in commercial batteries and related to both applied current rate and temperature, the conditions of battery use can be adjusted to extend lifetime and performance. Recently, *in operando* NPD studies of $LiFePO_4$ and V-doped $LiFePO_4$ cathodes [35] in large-format commercial cells have revealed a slightly more uniform phase-evolution during the charge/discharge processes in the doped material than in the pure one. This suggests that the onset and evolution of the phase transformation in the electrode can be manipulated by chemical doping. A multivariate approach to *in situ* NPD experiments of $LiFePO_4$ containing batteries was also undertaken to extract further detail from such experiments [49]. Using *in situ* NPD analysis of custom-made batteries, the phase evolution of $LiFePO_4$ cathodes was found to possess solid-solution regions, two-phase and simultaneous two-phase, as well as solid-solution behavior during cycling. Therefore, *in situ/operando* NPD has contributed to the understanding of the $LiFePO_4$ cathode function. However, minimal *in situ* data for $LiFePO_4$ (or any other electrode) at elevated temperature exists. Here, we present *in operando* NPD analysis of the $LiFePO_4/FePO_4$ phase evolution within a commercial battery at various applied current rates and temperature, which is directly correlated to the measured voltage.

2. Experimental

A commercial prismatic battery of dimensions 50 × 40 × 5 mm and containing a $LiFePO_4$ positive electrode was fabricated at Zhongzhi Power Co. Ltd., Zhejiang, China. The battery underwent three full cycles at low current (0.25 A) to ensure facile formation of a solid-electrolyte interface layer on both electrodes, and was charged to ~50–60% prior to the *in operando* experiment. The battery components included: aluminium casing, aluminium and copper current collectors, a graphite negative electrode, positive electrode mixture composed of polyvinyldifluoride (PVDF) with carbon black and $LiFePO_4$, and electrolyte composed of $LiPF_6$ dissolved in a 1:1 vol % of ethylene carbonate and dimethyl carbonate.

In operando NPD data were collected on WOMBAT, the high-intensity neutron powder-diffractometer, at the OPAL reactor facility at ANSTO [51]. The battery was placed in a neutron beam of wavelength (λ) = 2.4122 (1) Å, determined using the NIST Al_2O_3 676 standard reference material, and data collected in the range $25 \leq 2\theta \leq 135°$ every 5 min for 45 h. NPD data correction, reduction, and visualization were undertaken using the program LAMP [52]. During the *in operando* NPD experiment the electrochemical cell was cycled under different conditions including galvanostatic (constant current) mode with applied current ranging from ±0.25–1 A, potentiostatic (constant voltage) mode, and current free mode using an Autolab potentiostat/galvanostat (PG302N).

Elevated temperature experiments were performed using a custom-designed furnace. Temperature control was achieved using infrared quartz lamps within a vacuum furnace containing a parabolic Al mirror using a Eurotherm 3216 controller to modulate power to the lamps. The battery had one face exposed directly to the heating elements and calibrated thermocouples were placed near the front and rear panels of the battery, with the front panel receiving the direct heat from the lamps. The front panel temperature (closer to the halogen lamps) was higher than the rear panel (up to 30 °C in fast ramps) and the control sensor was placed at the warmest point. The set-point temperature was 405, 353, and 333 K at various points during the experiment. The control sensor took 50 min to reach 405 K after which it was kept at 405 K for 15 min, while the remaining temperature changes took 5 min with the temperature maintained afterwards for ~200 min.

Rietveld refinements using the *in operando* NPD data were carried out using the GSAS [53] suite of programs with the EXPGUI [54] interface.

3. Results and discussion

3.1. Initial characterisation

The battery is composed of electrolyte solution, separator, casing material, aluminum and copper current collectors, and the electrodes. Fig. 1a shows the first NPD pattern in the *in operando* series and Fig. 1b the calculated refinement profile using the NPD data with structural models of Li_xC_6 (lithiated graphite), $LiFePO_4$, $FePO_4$, Cu, and Al. The rate performance, charge/discharge curves at different applied currents, and the capacity as a function of cycle number are shown in Fig. 1c and d on cells tested offline.

3.2. Phase evolution

During battery function lithium-ions are transferred between the positive and negative electrodes, resulting in structural changes in the materials that are captured in the time-resolved NPD powder diffraction data [22,24,55] via changes in reflection intensity and 2θ position. Initial observation of the phase evolution of battery components as a function of electrochemical conditions and temperature can be made from examining contour plots of the time-resolved NPD data. Fig. 2a shows a selected region of the *in operando* NPD data as a contour-plot, where 2θ is shown along the x axis and time along the y, and intensity shown in color with the defined scale. The 2θ range is chosen to provide a clear visual illustration of reflections from $LiFePO_4$ and $FePO_4$ and their evolution during charge/discharge. At ~900 min the background increases from ~7000 to ~7500 counts as indicated in Fig. 2a. Re-scaling the higher background region of these data shows further detail concerning the phase evolution of the battery components (Fig. 2b).

3.3. $LiFePO_4$

The focus of this study is to explore the temperature and current rate behavior of the $LiFePO_4$ electrode structure. Typically, $LiFePO_4$ undergoes a two-phase transition during battery charge, converting

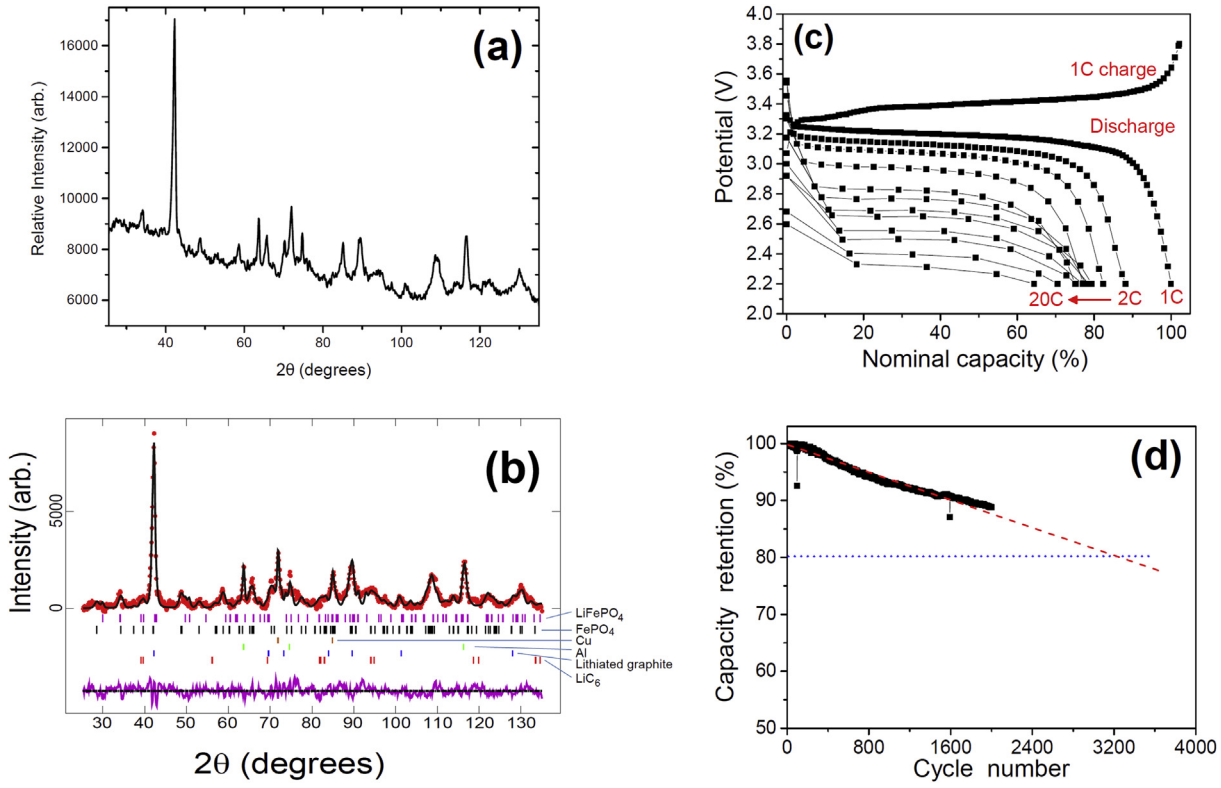

Fig. 1. a) The first NPD data collected during the *in operando* NPD experiment. **b)** The Rietveld refinement profile using data in (a), where data are red crosses and the calculation is shown in black and the difference between the two in purple. Vertical lines are Bragg reflection markers for the various battery phases as identified. Figures of merit are the profile factor (R_p) = 1.98%, weighted profile factor (wR_p) = 2.53%, and the goodness-of-fit term (χ^2) = 2.20. **c)** The charge and discharge curves at 1C where C refers to a charge process, in this case transfer of 1 Li^+ in 1 h. Discharge curves for higher C rates are also shown. **d)** The change in capacity as a function of cycle number with 1C cycles. (For interpretation of the references to colour in this figure legend, the reader is referred to the web version of this article.)

to $FePO_4$, and then back to $LiFePO_4$ by the same mechanism during discharge [4]. $LiFePO_4$ electrodes can undergo other reaction mechanisms and sequences, and intermediate phases have been identified during battery function at high rates [7,10,11,13,15–17,56]. Overall, the reaction mechanism and presence of reaction intermediates of $LiFePO_4$ depends on the particle size and morphology, as well as current [15,16]. The electrode studied here undergoes a two-phase reaction, where the $LiFePO_4$ reflections decrease in intensity, alongside increasing intensity of $FePO_4$ reflections, as shown by the reflections labelled in Fig. 2b. However, as discussed later, the onset of this phase transition with respect to the battery's electrochemical state and its evolution are unusual. We note that in addition to the two-phase reactions, reflections of the negative electrode change position, indicating a solid-solution reaction, in addition to two-phase reactions [21,27,57,58], with this behavior changing with the battery state of charge.

As the majority of the positive electrode reaction was found to be two-phase, during the sequential Rietveld refinement of $LiFePO_4$ and $FePO_4$ structures using these data, the lattice parameters of both phases were kept constant. Phase fractions were refined over the course of the charge/discharge of the battery, and the relative abundance of the positive electrode phases is shown along with the potential profile, applied current, and temperature, for the entire experiment in Fig. 3.

The rate of change of phase fractions was determined by a linear fit to the phase fraction evolution over the specified temporal region. The electrochemical-structural parameters explored over the course of the experiment, battery voltage, and the resultant $LiFePO_4$ and $FePO_4$ phase evolution rate, are described in Table 1. A wealth of information is available from such experiments that enable the relationship between battery performance, phase composition, and external conditions to be established. Below we discuss some findings with respect to the $LiFePO_4$ and $FePO_4$ phase fraction evolution.

3.4. Initial $LiFePO_4$ – $FePO_4$ evolution

The initial cycling conditions and phase evolution are shown in Fig. 4. At relatively low applied currents of 0.1 A during charge, the phase fraction of $LiFePO_4$ decreases linearly while the $FePO_4$ phase fraction increases, as expected. Thus, lower current charging appears to show an effectively linear phase change during charge.

3.5. An abrupt increase in temperature

A sharp rise in temperature appears to be detrimental to the battery as evidenced by the potential curve which varied significantly following the temperature step. For example, rather than the expected smooth potential plateau or plateau-like feature, spikes and rough plateau-like features are observed following the temperature increase. Notably, the first abrupt increase in temperature results in an increase in the background of the NPD patterns from ~7000 to 7500 counts, which persists throughout the remainder of the experiment even though the temperature was reduced to room temperature at various points during the experiment. This suggests that the initial temperature ramp caused an irreversible change.

3.6. Room temperature behavior following elevated temperature and high-current application

Next, we consider the 1230–2140 min region which corresponds to room temperature electrochemical behavior of $LiFePO_4$/

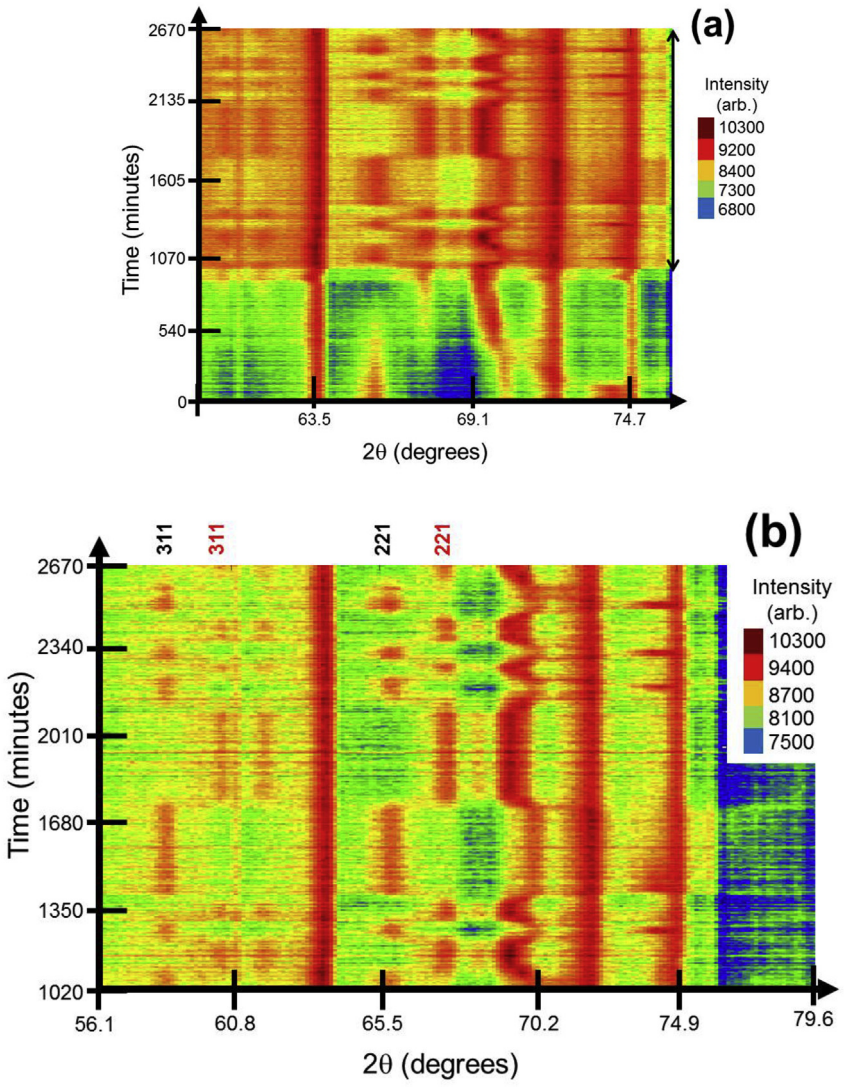

Fig. 2. **a)** A contour plot of *in operando* NPD data shown in a selected 2θ range (56–79°) composed of 534 NPD patterns that are stacked along the y-axis (time). **b)** Re-scaled region corresponding to the period of time following the application of a heating step. The $LiFePO_4$ and $FePO_4$ 311 and 221 reflections are labelled in black and red, respectively. (For interpretation of the references to colour in this figure legend, the reader is referred to the web version of this article.)

$FePO_4$ following elevated temperature. Fig. 5 shows the current, potential, and phase fraction evolution. We note that prior to this period, high charge/discharge rates were applied in addition to the two temperature steps shown in Fig. 3. Here, the phase evolution is somewhat unexpected, with the $LiFePO_4$ to $FePO_4$ transition on charge occurring near the end of charge. Additionally, there is a lag in the transformation, with $FePO_4$ appearing at the end of the charge and persisting into the discharge. Similarly the $FePO_4$ to $LiFePO_4$ transition occurs at the final stages of discharge and the transformation persists in the subsequent charge step. The collated NPD patterns and potential profile in Fig. 6 show this behavior, where arrows indicate the end of charge or discharge and shaded regions illustrate the phase dominance by $LiFePO_4$ in grey and $FePO_4$ in red. It is interesting to note that the phase evolution lag occurs in steps where no current is applied to the battery (i.e., the transformation continues during rest periods).

Describing the behavior in more detail, during the first charge in this region there is an unexpected increase in the $LiFePO_4$ phase fraction, occurring until close to the end of the charge where the $FePO_4$ phase fraction begins to increase (see Fig. 5). Subsequently, the $FePO_4$ phase continues to increase, stabilizing after the removal of current. During the following application of a discharge current, the phase fractions of both $LiFePO_4$ and $FePO_4$ remain essentially constant until the end of the discharge where the $LiFePO_4$ phase fraction increases rapidly and the $FePO_4$ fraction decreases. Again, with no current applied to the battery, the $LiFePO_4$ fraction continues to increase and then stabilize. The complete stabilization of the phase fractions in the zero-current regime occurs after 205 min (~68% into the regime). On application of a charge current the phase fractions remain stable until near the end of the charge where the $LiFePO_4$ fraction drops dramatically while the $FePO_4$ fraction increases. The phase fraction stabilizes in the first ~28% of the following zero-current regime. The transformation from $LiFePO_4$ to $FePO_4$ occurs near the end of the charge, and the phase change persists into the subsequent step. Therefore, depending on the battery history, the time taken for the transformation to conclude with a zero-current step varies, e.g., discharge at 1 A takes 205 min while charge at 0.75 A takes 50 min to achieve phase fraction stabilization in the adjacent zero-current regime.

A delay in the reaction evolution with respect to charge/discharge has been observed previously [50] and attributed to an inhomogeneous reaction across the electrode. This is

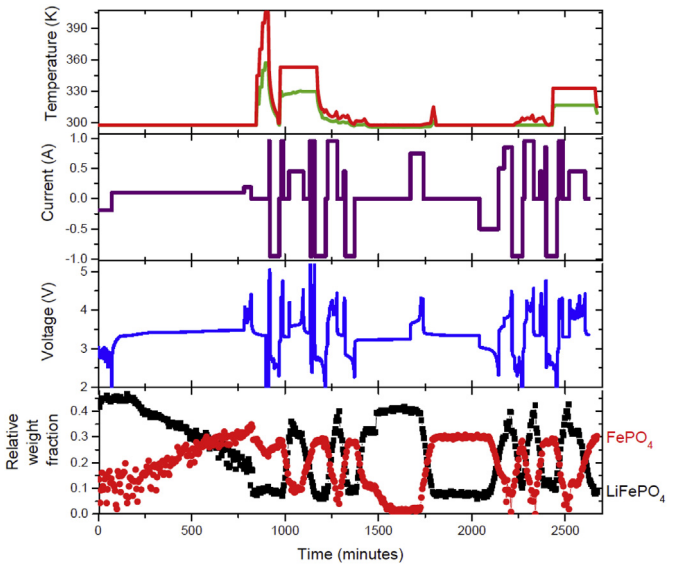

Fig. 3. The evolution of the $LiFePO_4$ (black) and $FePO_4$ (red) relative weight fraction, along with the measured voltage (blue), applied current (purple), and temperature of the battery at the surface closest to (red) and at the other side (green) of the halogen lamps. (For interpretation of the references to colour in this figure legend, the reader is referred to the web version of this article.)

predominantly related to the volume probed by the incident beam (X-rays) not representing the entire electrode. We note that in the present experiment the neutron beam probes at least half of the prismatic battery, resulting in data that represent the bulk average structure.

3.7. Rapid cycling following the temperature steps

In operando NPD is sensitive to the bulk transformation of the positive electrode where the majority of the battery is exposed to the neutron beam. The apparent initiation of the phase change illustrates that the majority of the positive electrode transforms near the end of charge (or discharge). This behavior may arise due to the applied temperature processes and the electrochemical cycling conditions. This phase-evolution behavior is further exaggerated by rapid cycling in the period following that shown in Fig. 5. When the current is changed sequentially from ±0.5 and ± 1 A (Fig. 7), on charge the $LiFePO_4$ phase increases until near the end of charge where it begins to drop rapidly and the $FePO_4$ fraction increases. Similarly, the $FePO_4$ phase increases during the subsequent discharge until near the end of discharge where it decreases rapidly and the $LiFePO_4$ phase increases. Thus, the phase expected to increase during the charge only does so in the last portion of charging and continues to increase during discharging and *vice versa*. This behavior differs significantly to the previously-observed virtually-uniform $LiFePO_4 \leftrightarrow FePO_4$ phase evolution occurring during charge/discharge [35]. Notably, beyond the short zero-current region following the charge step, ~2340 min, there is a continued decrease in the $LiFePO_4$ phase fraction and concomitant increase in the $FePO_4$ phase fraction. Hence, the lag in the phase evolution previously noted also occurs at higher current.

3.8. Comparison with the initial $LiFePO_4 - FePO_4$ evolution

The question arises whether the abnormalities observed in the $LiFePO_4$ phase-evolution are as a consequence of the temperature/current steps applied. The initial cycling conditions and phase evolution are shown in Fig. 4 and at low applied currents of 0.1 A during charge, the $LiFePO_4$ phase fraction decreases linearly while the $FePO_4$ phase fraction increases. We note that this occurs during, rather than at the end of, the charge. Heat is applied at ~845 min (indicated by the arrow) in conjunction with a current increase necessary due to experimental time constraints. Although, the lower-current initial charging results in an effectively-linear phase evolution during charge, after the temperature/current increase the majority of the phase evolution occurs near the end of the charge or discharge. The phase evolution continues somewhat into neighbouring electrochemical steps, as observed almost immediately after the temperature/higher-current step in the discharge finishing at 970 min. Here the $FePO_4$ phase fraction drops and the $LiFePO_4$ phase fraction increases rapidly near the end of the process, initiating the apparent lag in the phase evolution.

3.9. Phase evolution rate

Linear fits were applied to temporal sections where an approximately linear evolution of the phase fractions were observed and these are presented in Table 1, enabling the rate of change to be compared under various conditions. Interestingly, the overall magnitude of phase evolution varies from 1 (1) $\times 10^{-4}$ to 6.6 (2) $\times 10^{-3}$ phase fraction/min for the majority of the processes with the exception of a few which are effectively 0 (e.g. 2040–2090 min), indicating an order of magnitude variation in the rate of phase fraction change during the experiment.

Considering the zero-current regimes, the first of these follows the current step of 0.2 A (825–910 min) and begins at the first temperature increase. This first regime has a rate of change of the phase fractions of 2–8 $\times 10^{-4}$ phase fraction/min (1100–1160 min) compared with that for the initial sections of the zero-current regimes (1375–1435 min) of ~1 $\times 10^{-3}$ phase fraction/min. This difference likely arises because of the higher current applied after the first zero-current (≥0.45 A) and temperature step. However, selected zero-current steps applied for longer periods instigate a drop in the rate of phase fraction change, to ~1 $\times 10^{-4}$ or 1 $\times 10^{-5}$ phase fraction/min (e.g. 1435–1485 min). This indicates that longer periods are required for the electrode to equilibrate and phase fractions stabilize under higher current or temperature.

Considering the charge process, previous work investigating electrode lattice evolution revealed that the rate of change of lattice parameters is proportionally correlated to the current [21,26]. In the present work, the magnitude of the rate of change of the phase fractions is not directly proportional to the current. For example, although doubling the current from 0.1 to 0.2A increases the rate of change of the phase fraction, the rate at 0.75 A (6.1 (6) $\times 10^{-3}$) is larger than at 0.95 A (0.0037 (3) $\times 10^{-4}$). Such unexpected trends likely arise from processes occurring in the previous electrochemical step, affecting the point in the charge/discharge process at which the majority of the phase evolution occurs. This in turn is thought to influence the rate of change of phase fraction reported in Table 1. Generally, discharge steps have a smaller rate of phase evolution compared to charge steps at similar applied currents, e.g. 1.6 (5) $\times 10^{-3}$ phase fraction/min on discharge compared to 5.4 (1) $\times 10^{-3}$ phase fraction/min on charge at ± 0.95 A. Therefore, we identify a faster rate of phase evolution of this electrode on charge than for discharge under the conditions probed in this study.

The phase evolution changes dramatically with the electrochemical and external conditions used in this study and reasons for this change are likely associated with the combination of temperature and current applied which speculatively could result in a distribution of particles in intimate contact with electrode matrix (e.g. carbon black) or separator while others lose this contact and thus the evolution is delayed in a proportion of particles. If part of the electrolyte turns gaseous (via internal hot spots) this could also

Table 1
Rate of change of $LiFePO_4$ and $FePO_4$ phase fraction and associated electrochemical and external parameters - current, temperature, voltage characteristics, and capacity. Shading represents charge (purple), zero applied current (orange), and discharge (blue).

Period (start and finish, min)	Rate of change of $LiFePO_4$ phase fraction (phase fraction/min)	Rate of change of $FePO_4$ phase fraction (phase fraction/min)	Current (A)	Temperature (K)	Time taken (min)	Voltage characteristics	Capacity (Ah)
1st charge (75 - 775)	-0.000377(6)	0.00033(1)	0.1	298(5)	700	3.4 V plateau	1.17
Application of a higher current (775 - 825)	-0.0006(5)	0.0008(1)	0.2	298(5)	50	Increasing V to specified cut-off	0.17
1st heat treatment with no applied current (825 - 910)	0.000248(7)	-0.00088((6)	0	Heating to 357(5) / 405(5)	85	Slow drop in V followed by a rapid loss	-
1st discharge while cooling (920 - 965)	-0.0001(1)	0.0005(2)	-1	Cooling to 300(5)	45	Continuing drop in V towards cut-off	0.75
2nd heat and maintained at elevated temperature with no applied current and 2nd slow and quick charge (976 - 1035)	0.0059(2)	-0.0038(2)	0, 0.45. 0.95	330(5) / 353(5)	123	Rapid increase to a 3.1 V plateau with a very slow decrease in V at 0 A and increase to 3.6 V at 0.45 A	0.11, 0.21
Elevated temperature and continuation of 2nd slow charge (1035 - 1095)	-0.0009(2)	0.0001(2)	0.45	330(5) / 353(5)	60	3.6 V plateau followed by increase to V cut-off	0.45
Elevated temperature with no current applied, the completion of the 2nd charge, and with current fluctuations (1100 - 1160)	-0.00324(7)	0.00228(9)	0, 0.95, -0.95, 0.95	330(5) / 353(5)	60	Drops to 3.4 V during 0 A, followed by V spikes	0.03, 0.16, 0.22
Cooling and 2nd quick discharge (1160 - 1220)	0.000009(140) ~0	0.000007(160) ~0	-0.95	Cooling from 330(5) to 305(5) / 353(5) to 313(5)	60	From 2.8 V dropping to V cut-off	0.95
Elevated temperature and 3rd quick charge (1220 - 1280)	0.0054(1)	-0.0037(1)	0.95	300(5) / 310(5)	60	Increasing V until cut-off	0.95
Elevated temperature and no applied current (1280 - 1320)	-0.0049(6)	0.0037(5)	0, 0.45	300(5) / 310(5)	40	Drops from 3.4 to 3.3 V after another small current/V spike	-
Cooling and 3rd quick discharge (1320 - 1370)	-0.0016(5)	0.0014(4)	-0.95	Cooling to 298(5)	30	From 2.8 V dropping to V cut-off	0.48
No applied current #1 (1375 - 1435)	0.0046(3)	-0.0031(2)	0	298(5)	60	Increases to 3.2 V and slowly increases	-
No applied current #2 (1435 - 1485)	-0.0001(1)	-0.0002(1)	0	298(5)	50	Increases by 0.01 V	-
No applied current #3 (1490 - 1560)	0.00010(3)	-0.0010(1)	0	298(5)	70	Increases by 0.004 V	-
No applied current #4 and 4th charge (1565 - 1725)	-0.00009(2)	0.00003(2)	0, 0.75	298(5)	160	Increases by 0.007 V and the 3.6 V and increasing	0.63
End of 4th charge (1725 - 1740)	-0.0052(5)	0.0061(6)	0.75	298(5)	15	From 3.8 V to cut-off	0.19
No applied current #5 (1740 - 1800)	-0.0042(2)	0.0032(1)	0	298(5) and 315(5)	60	From 3.56 V to 3.36	-
No applied current #6 (1800 - 2040)	-0.00001(1)	0.000014(6)	0	298(5)	240	Drop off of 0.021 V	
4th discharge (2040 - 2090)	0.00003(11)	-0.00001(6)	-0.5	298(5)	50	3 V plateau	0.42
4th discharge continued (2090 - 2140)	0.0027(2)	-0.00229(9)	-0.5	298(5)	50	Drops to cut-off	0.42
5th charge (2140 - 2170)	0.0030(2)	-0.0014(1)	0.5	298(5)	30	Increase and stabilises ~ 3.54 V	0.25
5th charge increased current (2170 - 2210)	0.0027(4)	-0.0021(9)	0.85	298(5)	40	Jump to 3.8 V and then increase to cut-off	0.56
5th discharge and a slight increase in temperature (2215 - 2270)	-0.0046(2)	0.0040(1)	-0.95	298(5) / 305(5)	55	To cut-off	0.87
6th charge and slightly elevated temperature (2270 - 2340)	0.0047(2)	-0.0037(3)	0.95, 0	298(5) / 305(5)	70	To cut-off	0.79
No applied current slightly elevated temperature (2340 - 2390)	-0.0059(4)	0.0052(4)	0, 0.45	298(5) / 305(5)	50	3.4 V plateau	-
6th discharge and slightly elevated temperature (2390 - 2450)	-0.0005(1)	0.00008(9)	0.85, -0.95	298(5) / 305(5) 315(5) / 330(5)	60	2.8 V drop to cut-off	0.87
Elevated temperature with no applied current and a short burst of current (2450 - 2520)	0.0047(3)	-0.0037(3)	0, 0.95	315(5) / 330(5)	70	3.3 V with no applied current and increase to V cut-off with applied current	-
Elevated temperature 7th charge short burst (2465 - 2485)	0.0066(2)	-0.0052(6)	0.95	315(5) / 330(5)	20	Increase to V cut-off	0.32
Elevated temperature 7th charge (2520 - 2540)	-0.005(2)	0.005(1)	0.45	315(5) / 330(5)	20	Between 4.0 and 3.7 V	0.15
Elevated temperature 7th charge (2540 - 2570)	0.0003(2)	-0.0003(1)	0.45	315(5) / 330(5)	30	Between 4.1 and 3.7 V	0.23
Elevated temperature 7th charge (2570 - 2605)	-0.0032(2)	0.0025(2)	0.45	315(5) / 330(5)	35	Between 4.2 and 3.7 V	0.26
No applied current to end (2605 - 2625)	-0.0033(1)	0.0022(2)	0	315(5) / 330(5)	20	Drops from 3.9 to 3.36 V	-

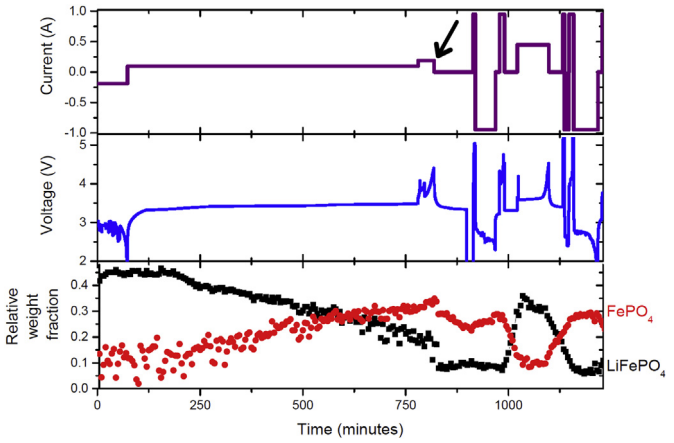

Fig. 4. Evolution of the $LiFePO_4$ (black) and $FePO_4$ (red) relative weight fraction, along with the measured voltage (blue) and applied current (purple) in the first temporal region. The arrow indicates where heat was applied. (For interpretation of the references to colour in this figure legend, the reader is referred to the web version of this article.)

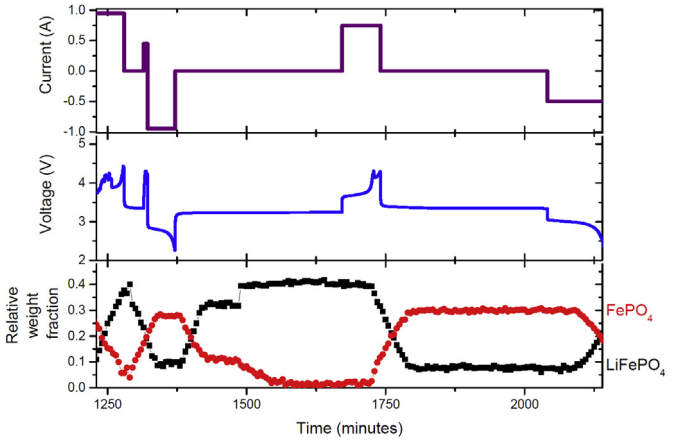

Fig. 5. Evolution of the $LiFePO_4$ (black) and $FePO_4$ (red) relative weight fraction, along with the measured voltage (blue) and applied current (purple) in a selected temporal region. (For interpretation of the references to colour in this figure legend, the reader is referred to the web version of this article.)

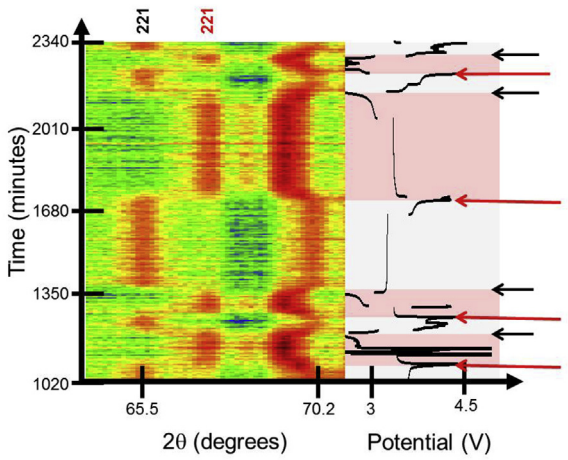

Fig. 6. Region of *in operando* NPD data showing the $LiFePO_4$ 221 (black) and $FePO_4$ 221 (red) reflections and the potential profile. Red arrows indicate the end of charge and black arrows indicate the end of discharge. Grey shading of the potential profile indicates $LiFePO_4$ dominance of the positive electrode and red shading indicates dominance by $FePO_4$. (For interpretation of the references to colour in this figure legend, the reader is referred to the web version of this article.)

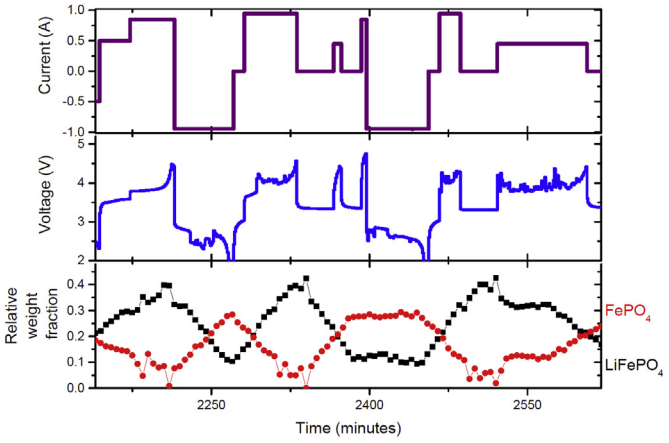

Fig. 7. The evolution of the $LiFePO_4$ (black) and $FePO_4$ (red) relative weight fraction, along with the measured voltage (blue) and applied current (purple) in the final temporal region. (For interpretation of the references to colour in this figure legend, the reader is referred to the web version of this article.)

result in poorer particle contacts. Delamination of the electrodes or particles may account for the structural response. These are speculative particle-level concepts of how the phase evolution can be modified. It is interesting to note that the evolution appears to finish (complete) before the reverse occurs, e.g. a lag, which may indicate sufficient energy exists in the system to force the completion of a two-phase reaction or at least a proportion of it even though the current is "opposing this mechanism". This can again speculatively be related to the cascade model [11,59] with the particles that are partially converted continuing to fully convert before nucleating the next phase. These concepts require extensive further characterisation in order to systematically define the most probable reason for the observed behavior.

This study represents the bulk evolution of the entire $LiFePO_4$ electrode during charge/discharge in a commercial prismatic battery. Recent work on coin-type equivalent cells between 253 and 333 K show the presence of intermediate phases between the $LiFePO_4$ and $FePO_4$ phases during charge/discharge with $LiFePO_4$/C that feature particle sizes of ~43 nm [60]. However, the reaction evolution upon charge and discharge was not explored in detail by these authors. Interestingly, in Fig. 1d–f and 2a–c of this work [60], the reflection evolution appears to show that the majority of the transformation from $LiFePO_4$ to $FePO_4$ (via the intermediate) occurs asymmetrically and closer to the end of charge or discharge (at 293 and 273 K) which was not discussed by the authors. We are able to assign this delay to temperature and applied current in our work, which may indeed play a role in the previous work. It should be noted that the X-ray beam in this work is unlikely to obtain information from the entire sample as it will be exposed to only a portion of the electrode, whereas with neutron diffraction, we are obtaining information from the majority of the battery. Further work using synchrotron X-ray microbeam diffraction has investigated rate-dependence of the $LiFePO_4$ to $FePO_4$ transformation based on individual grains [61]. These authors observe a delay or the converse in phase transformation at certain applied currents in addition to asymmetric evolution but this is deemed to be related to the number of grains probed and the measurement condition. The transformation is also shown to be rate dependent, larger applied current resulting in shorter transformation times. In addition, due to the shorter discharge/charge times with larger applied

current a greater proportion of grains are active. The grain level picture is virtually a small picture to what is being detected by *in operando* neutron powder diffraction. Thus there is some preliminary evidence of reaction evolution modification with current and/or temperature but this has not been characterised in detail.

This initial study shows the power of *in operando* NPD to explore current and temperature dependent electrode behavior in commercial batteries. Future work will take a more systematic approach to investigate and de-convolute the effects of temperature and current, and is expected to shed further light on the reaction evolution and relationship to current, temperature, and battery history.

4. Conclusions

We report for the first time the temperature and current-dependent structural evolution of the $LiFePO_4$ positive electrode within a commercial battery using *in operando* neutron powder diffraction (NPD). We show that a higher temperature step irreversibly affects the battery and influences the $LiFePO_4$ phase evolution. The application of high current and temperature drives the $LiFePO_4$ to $FePO_4$ phase evolution to occur near the end charge and into subsequent electrochemical processes. This is clearly evident when zero current steps are applied and is exaggerated during continuous charge/discharge steps. Such data shows that the electrode is not in equilibrium and that time beyond the end of the charge or discharge indicated by the battery state of charge is required for transformation to the anticipated phase. *In operando* NPD experiments provide insight into the phase evolution of the $LiFePO_4$ electrode during the charge or discharge process, and this is particularly important following heating or high current. The information regarding the phase evolution will allow the performance of these batteries in high-power applications such as electric vehicles, which may undergo thermal steps and variable current rate cycling, to be improved.

Acknowledgements

The infrastructure and materials for the experiments were in part provided by the Functional Materials for Energy Systems and Devices research project within the Australian Centre for Neutron Scattering. Dr Sharma would like to acknowledge the Australian Research Council via the DECRA scheme (DE160100237).

References

[1] T. Nagaura, K. Tozawa, Prog. Batter. Sol. Cells 9 (1990) 209.
[2] J.-M. Tarascon, M. Armand, Nature 414 (2001) 359–367.
[3] M.M. Thackeray, A. de Kock, M.H. Rossouw, D. Liles, R. Bittihn, D. Hoge, J. Electrochem. Soc. 139 (1992) 363–366.
[4] A.K. Padhi, K.S. Nanjundaswamy, J.B. Goodenough, J. Electrochem. Soc. 144 (1997) 1188–1194.
[5] S.Y. Chung, J.T. Bloking, Y.M. Chiang, Nat. Mater. 1 (2002) 123–128.
[6] N. Sharma, M.V. Reddy, G. Du, S. Adams, B.V.R. Chowdari, Z. Guo, V.K. Peterson, J. Phys. Chem. C 115 (2011) 21473–21480.
[7] P. Gibot, M. Casas-Cabanas, L. Laffont, S. Levasseur, P. Carlach, S. Hamelet, J.-M. Tarascon, C. Masquelier, Nat. Mater. 7 (2008) 741–747.
[8] N. Ravet, A. Abouimrane, M. Armand, Nat. Mater. 2 (2003) 702s.
[9] H. Huang, S.C. Yin, L. Nazar, Electrochem. Solid-State Lett. 4 (2001) A170–A172.
[10] P. Bai, D.A. Cogswell, M.Z. Bazant, Nano Lett. 11 (2011) 4890–4896.
[11] C. Delmas, M. Maccario, L. Croguennec, F. Le Cras, F. Weill, Nat. Mater. 7 (2008) 665–671.
[12] L. Laffont, C. Delacourt, P. Gibot, M.Y. Wu, P. Kooyman, C. Masquelier, J.-M. Tarascon, Chem. Mater. 18 (2006) 5520–5529.
[13] N. Sharma, X. Guo, G. Du, Z. Guo, J. Wang, Z. Wang, V.K. Peterson, J. Am. Chem. Soc. 134 (2012) 7867–7873.
[14] M. Wagemaker, D.P. Singh, W.J.H. Borghols, U. Lafont, L. Haverkate, V.K. Peterson, F.M. Mulder, J. Am. Chem. Soc. 133 (2011) 10222–10228.
[15] Y. Orikasa, T. Maeda, Y. Koyama, H. Murayama, K. Fukuda, H. Tanida, H. Arai, E. Matsubara, Y. Uchimoto, Z. Ogumi, J. Am. Chem. Soc. 135 (2013) 5497–5500.
[16] H. Liu, F.C. Strobridge, O.J. Borkiewicz, K.M. Wiaderek, K.W. Chapman, P.J. Chupas, C.P. Grey, Science 344 (2014) 1252817.
[17] X. Zhang, M. van Hulzen, D.P. Singh, A. Brownrigg, J.P. Wright, N.H. van Dijk, M. Wagemaker, Nano Lett. 14 (2014) 2279–2285.
[18] N. Sharma, W.K. Pang, Z. Guo, V.K. Peterson, ChemSusChem 8 (2015) 2826–2853.
[19] V.K. Peterson, C.M. Papadakis, IUCrJ 2 (2015) 292–304.
[20] W.R. Brant, S. Schmid, G. Du, H.E.A. Brand, W.K. Pang, V.K. Peterson, Z. Guo, N. Sharma, J. Vis. Exper. 93 (2014) 52284.
[21] N. Sharma, V.K. Peterson, Electrochim. Acta 101 (2013) 79–85.
[22] N. Sharma, V.K. Peterson, J. Solid State Electrochem. 16 (2012) 1849–1856.
[23] M. Alam, T. Hanley, W.K. Pang, V.K. Peterson, N. Sharma, Powder Diffr. 29 (2014) S35–S39.
[24] N. Sharma, V.K. Peterson, M.M. Elcombe, M. Avdeev, A.J. Studer, N. Blagojevic, R. Yusoff, N. Kamarulzaman, J. Power Sources 195 (2010) 8258–8266.
[25] X.-L. Wang, K. An, L. Cai, Z. Feng, S.E. Nagler, C. Daniel, K.J. Rhodes, A.D. Stoica, H.D. Skorpenske, C. Liang, W. Zhang, J. Kim, Y. Qi, S.J. Harris, Sci. Rep. 2 (2012) 1–7.
[26] N. Sharma, D. Yu, Y. Zhu, Y. Wu, V.K. Peterson, Chem. Mater. 25 (2013) 754–760.
[27] N. Sharma, V.K. Peterson, J. Power Sources 244 (2013) 695–701.
[28] J.-F. Colin, V. Godbole, P. Novák, Electrochem. Comm. 12 (2010) 804–807.
[29] G. Du, N. Sharma, J.A. Kimpton, D. Jia, V.K. Peterson, Z. Guo, Adv. Funct. Mater. 21 (2011) 3990–3997.
[30] W.K. Pang, V.K. Peterson, N. Sharma, J.-J. Shiu, S.H. Wu, Chem. Mater. 26 (2014) 2318–2326.
[31] W.K. Pang, V.K. Peterson, N. Sharma, J.-J. Shiu, S.H. Wu, Powder Diffr. 29 (2014) S59–S63.
[32] J. Li, R. Petibon, S. Glazier, N. Sharma, W.K. Pang, V.K. Peterson, J.R. Dahn, Electrochim. Acta 180 (2015) 234–240.
[33] R. Petibon, J. Li, N. Sharma, W.K. Pang, V.K. Peterson, J.R. Dahn, Electrochim. Acta 174 (2015) 417–423.
[34] O. Dolotko, A. Senyshyn, M.J. Muhlbauer, K. Nikolowski, F. Scheiba, H. Ehrenberg, J. Electrochem. Soc. 159 (2012) A2082–A2088.
[35] C.-W. Hu, N. Sharma, C.-Y. Chiang, H.-C. Su, V.K. Peterson, H.-W. Hsieh, Y.-F. Lin, W.-C. Chou, B.-Y. Shew, C.-H. Lee, J. Power Sources 244 (2013) 158–163.
[36] H. Liu, C.R. Fell, K. An, L. Cai, Y.S. Meng, J. Power Sources 240 (2013) 772–778.
[37] O. Dolotko, A. Senyshyn, M.J. Muhlbauer, K. Nikolowski, H. Ehrenberg, J. Power Sources 255 (2014) 197–203.
[38] W.K. Pang, M. Alam, V.K. Peterson, N. Sharma, J. Mater. Res. 30 (2015) 373–380.
[39] W.K. Pang, S. Kalluri, V.K. Peterson, S.X. Dou, Z. Guo, Phys. Chem. Chem. Phys. 16 (2014) 25377–25385.
[40] H. Berg, H. Rundlov, J.O. Thomas, Solid State Ionics 144 (2001) 65–69.
[41] O. Bergstom, A.M. Andersson, K. Edstrom, T. Gustafsson, J. Appl. Cryst. 31 (1998) 823–825.
[42] M. Bianchini, J.B. Leriche, J.-L. Laborier, L. Gendrin, E. Suard, L. Croguennec, C. Masquelier, J. Electrochem. Soc. 160 (2013) A2176–A2183.
[43] V.A. Godbole, M. Hess, C. Villevieille, H. Kaiser, J.F. Colin, P. Novak, RSC Adv. 3 (2013) 757–763.
[44] N. Sharma, G. Du, A.J. Studer, Z. Guo, V.K. Peterson, Solid State Ionics 199–200 (2011) 37–43.
[45] W.K. Pang, V.K. Peterson, J. Appl. Cryst. 48 (2015) 280–290.
[46] M. Bianchini, F. Fauth, E. Suard, J.B. Leriche, C. Masquelier, L. Croguennec, Acta. Cryst. 71 (2015) 688–701.
[47] S. Taminato, M. Yonemura, S. Shiotani, T. Kamaiyama, S. Torii, M. Nagao, Y. Ishikawa, K. Mori, T. Fukunaga, Y. Onodera, Y. Naka, M. Morishima, Y. Ukyo, D.S. Adipranoto, H. Arai, Y. Uchimoto, Z. Ogumi, K. Suzuki, M. Hirayama, R. Kanno, Sci. Rep. 6 (2016) 28843.
[48] J. Jones, J.-T. Hung, Y.S. Meng, J. Power Sources 189 (2009) 702–705.
[49] M.A. Rodriguez, M.H. Van Benthem, D. Ingersoll, S.C. Vogel, H.M. Reiche, Powder Diffr. 25 (2010) 143–148.
[50] H.H. Chang, C.C. Chang, H.C. Wu, M.H. Yang, H.S. Sheu, N.L. Wu, Electrochem. Commun. 10 (2008) 335–339.
[51] A.J. Studer, M.E. Hagen, T.J. Noakes, Phys. B 385–386 (2006) 1013–1015.
[52] D. Richard, M. Ferrand, G.J. Kearley, J. Neutron Res. 4 (1996) 33–39.
[53] A.C. Larson, R.B. Von Dreele, in: Los Alamos National Laboratory Report LAUR 86-748, 1994.
[54] B.H. Toby, J. Appl. Cryst. 34 (2001) 210–213.
[55] M. Winter, J.O. Besenhard, M.E. Spahr, P. Novak, Adv. Mater. 10 (1998) 725–763.
[56] C. Delacourt, P. Poizot, J.-M. Tarascon, C. Masquelier, Nat. Mater. 4 (2005) 254–260.
[57] J.R. Dahn, Phys. Rev. B 44 (1991) 9170–9177.
[58] L.B. Ebert, Annu. Rev. Mater. Sci. 6 (1976) 181–211.
[59] G. Brunetti, D. Robert, P. Bayle-Guillemaud, J.L. Rouviere, E.F. Rauch, J.F. Martin, J.F. Colin, F. Bertin, C. Cayron, Chem. Mater. 23 (2011) 4515–4524.
[60] M. Yan, G. Zhang, Q. Wei, X. Tian, K. Zhao, Q. An, L. Zhou, Y. Zhao, C. Niu, W. Ren, L. He, L. Mai, Nano Energy 22 (2016) 406–413.
[61] X. Zhang, M. Van Hulzen, D.P. Singh, A. Brownrigg, J.P. Wright, N.H. Van Dijk, M. Wagemaker, Nat. Commun. 6 (2015) 8333.